


Article

Strength Behaviors of Remolded Hydrate-Bearing Marine Sediments in Different Drilling Depths of the South China Sea

Yanghui Li ¹, Tingting Luo ^{1,*}, Xiang Sun ¹, Weiguo Liu ¹, Qingping Li ², Yuanping Li ³ and Yongchen Song ^{1,*}

¹ Key Laboratory of Ocean Energy Utilization and Energy Conservation of Ministry of Education, Dalian University of Technology, Dalian 116024, China; liy@dlut.edu.cn (Y.L.); shyaansun@outlook.com (X.S.); liuwg@dlut.edu.cn (W.L.)

² China National Offshore Oil Corporation, Beijing 100010, China; liqp@cnooc.com.cn

³ China National Offshore Oil Corporation, Shenzhen 518068, China; LiYP5@cnooc.com.cn

* Correspondence: ligongltt@mail.dlut.edu.cn (T.L.); songyc@dlut.edu.cn (Y.S.)

Received: 29 November 2018; Accepted: 11 January 2019; Published: 15 January 2019



Abstract: The mechanical behaviors of hydrate-bearing marine sediments (HBMS) drilled from the seafloor need to be understood in order to safely exploit natural gas from marine hydrate reservoirs. In this study, hydrates were prepared using ice powder and CH₄ gas, and HBMS from the Shenhu area in the South China Sea were remolded using a mixed sample preparation method. A series of triaxial tests were conducted on the remolded HBMS to investigate the effects of soil particle gradation and the existence of hydrate on the mechanical properties of hydrate reservoirs. The results show that the stiffness and failure strength of HBMS decrease along with the decrease of mean particle size and soil aggregate morphology change at different drilling depths, and the reduction of failure strength is more than 20% when the drilling depth drops by 30 m. A better particle gradation of marine sediments may boost the stiffness and failure strength of HBMS. In addition, the existence of hydrate plays an important role in the strength behaviors of HBMS. The reduction of failure strength of HBMS with 30% initial hydrate saturation is more than 35% after complete hydrate dissociation.

Keywords: hydrate-bearing marine sediments; South China Sea; failure strength; soil particle gradation; existence of hydrate; hydrate dissociation

1. Introduction

Methane gas hydrate, an ice-like compound, has attracted the attention of global scientists for its huge exploitation potential [1–5]. In recent years, a series of research projects on gas hydrate have been carried out in China, Japan, the United States of America and India [6–9]. Many marine explorations have confirmed that large amounts of natural gas hydrate resources exist in the Shenhu area in the South China Sea [10–12]. Thus, this area may become an objective target for hydrate exploitation in the future. However, hydrate dissociation in the natural gas exploitation process may lead to submarine landslides and tsunamis, and further give rise to unexpected engineering facility damage [13–18]. Hence, the mechanical behaviors of HBMS need to be investigated systematically before that the large-scale exploitation from gas hydrate reservoirs is undertaken.

Up to now, a series of experimental studies on artificial hydrate-bearing sediments have been conducted systematically in the laboratory [19–35]. It has been proven that the confining pressure, sediment matrix, hydrate saturation and hydrate type have significant influences on the failure strength, stiffness and volume characteristics of hydrate-bearing sediments [9,36–44].

More importantly, some triaxial tests on HBMS drilled from the seafloor have been carried out for investigation. Masui et al. [45,46] firstly conducted a series of triaxial shear tests on the HBMS drilled from offshore Japan and found that when the particle size distributions of hydrate-bearing sands are close to that of remolded HBMS, the strength properties and deformation characteristics of these two materials are consistent. Yoneda et al. [43] found that HBMS containing different fine contents display different E50 modulus due to the better mobility of fine particles in that material during the shear process. Winters et al. [47] then conducted a series of drained and undrained triaxial tests on hydrate cores drilled from the Krishna-Godavari and Mahanadi Basins located offshore from India, and they found that fine-grained HBMS obviously exhibits shear shrinkage behaviors while sandy HBMS displays a higher internal friction angle. These research described above suggests that the particle size of marine sediments has a significant influence on the mechanical characteristics of HBMS.

Hyodo et al. [48,49] confirmed that the failure strength of remolded HBMS from the Nankai Trough located offshore from Japan increases with the increase of effective confining pressure. The internal friction angle and cohesion force significantly reflect the mechanical properties of that material. After that, Yoneda et al. [9,43,50] studied the mechanical behaviors of HBMS from the Daini-Atsumi Knoll located offshore from Japan and found that the peak friction angle of that material would drop by 30% after hydrate dissociation. Luo et al. [51] proved that the failure strength of remolded HBMS of the South China Sea increases with the increase of confining pressure and shows an obvious reduction after hydrate dissociation. Priest et al. [52] and Yun et al. [53] pointed out that hydrate dissociation induced by the production of gas hydrates within under-consolidated sediments may potentially lead to seafloor instability based on the mechanical property investigation of HBMS from the Krishna–Godavari Basin, offshore from India. All of the above research demonstrates that the existence of hydrate plays an important role in the mechanical properties of HBMS. However, to date, studies published focusing on remolded HBMS of the South China Sea are still rare. Investigations have shown that hydrate cores drilled from the South China Sea are predominantly composed of fine-grained particles, and silty-size particles count for approximately 50% [51,54], which differs from the sediment matrix of other hydrate reservoirs. Moreover, the particles size of the sediment matrix has a significant influence on the mechanical properties of hydrate reservoirs [46,55,56]. It is important to understand the mechanical behaviors of remolded HBMS of the South China Sea to assess the risk of hydrate exploitation and exploration.

In this study, hydrates were prepared using ice powder and CH₄ gas. HBMS from the Shenhu area in the South China Sea were remolded using a mixed sample preparation method. The stress–strain behaviors, elastic modulus and failure strength of HBMS, hydrate-bearing artificial silt and hydrate-bearing kaolin clay were obtained and intercompared to study the effect of soil particle gradation on the mechanical properties of reservoirs. In addition, the mechanical behaviors of HBMS after hydrate dissociation were studied, and several triaxial tests on HBMS with different hydrate saturations and different existence forms of hydrate (uniform distribution and interbedded) were also conducted to understand the effect of existence of hydrate on the mechanical properties of HBMS.

2. Experimental Methods

2.1. Apparatus

In this study, all the HBMS were sheared by a triaxial apparatus (TAW-60, Chaoyang Test Instrument Co. Ltd., Changchun, China), and a schematic diagram of the triaxial testing system is shown in Figure 1. This triaxial apparatus consists of four systems: an axial loading system, a temperature control system, a confining pressure servo system and a computer control system. The function of the axial loading system is to provide axial pressure to the sample with a normal loading capacity of 60 kN with a pressure precision of 0.01 kN by an axial servo motor and a removable piston. The temperature control system can ensure the temperature of the pressure chamber ranging from −30 °C to 30 °C with a precision of 0.1 °C, using a thermostatic bath and an internal heat

exchanger around the sample. The confining pressure servo system provides a confining pressure with a maximum of 30 MPa and a pressure precision of 0.01 MPa by a plunger pump. The data acquisition and the experimental parameter setup are accomplished by computer control system, which consists of the control software entitled “Test”, a full digital servo controller (DOLI Elektronik Co. Ltd., Munich, Germany), a pressure transducer and a temperature transducer.

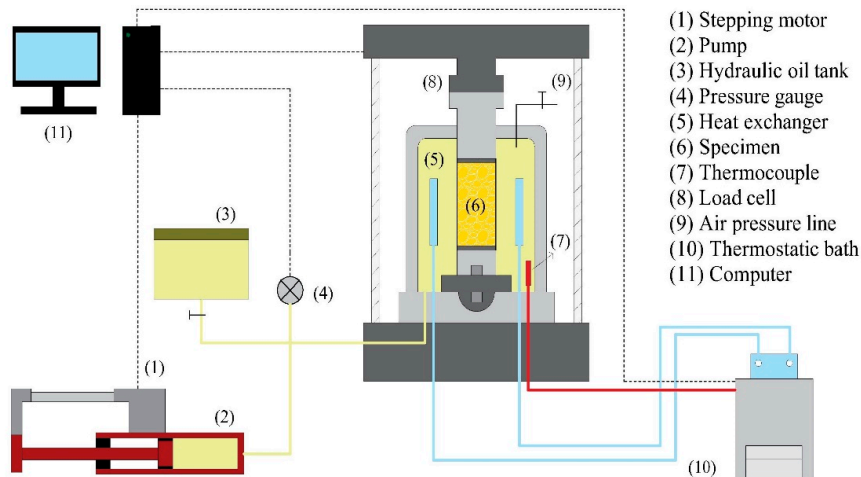


Figure 1. Schematic diagram of the triaxial testing system

2.2. Marine Sediments

The marine sediments were obtained from the Shenhu area in the South China Sea. At a water depth of about 1200 m, the drilling depth of marine sediments ranges from 128 m to 158 m. The results also show that the hydrate saturation varies from 20% to 40%, and the permeability is lower than 10 mD. The temperature of the seafloor is about 3.75 °C and the geothermal gradient is about 0.0045 °C/m. Figure 2 shows the appearance of marine sediments before and after remolding.

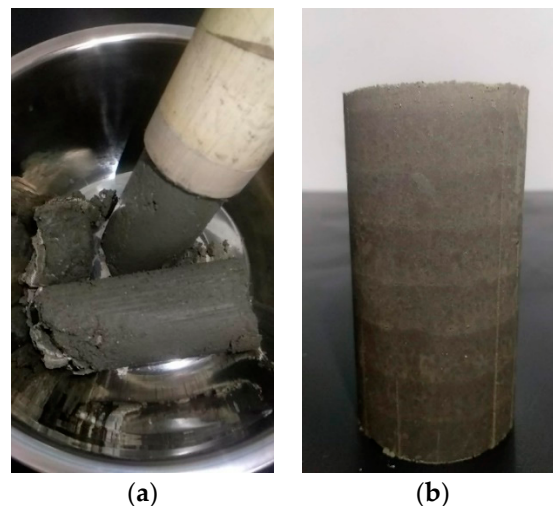


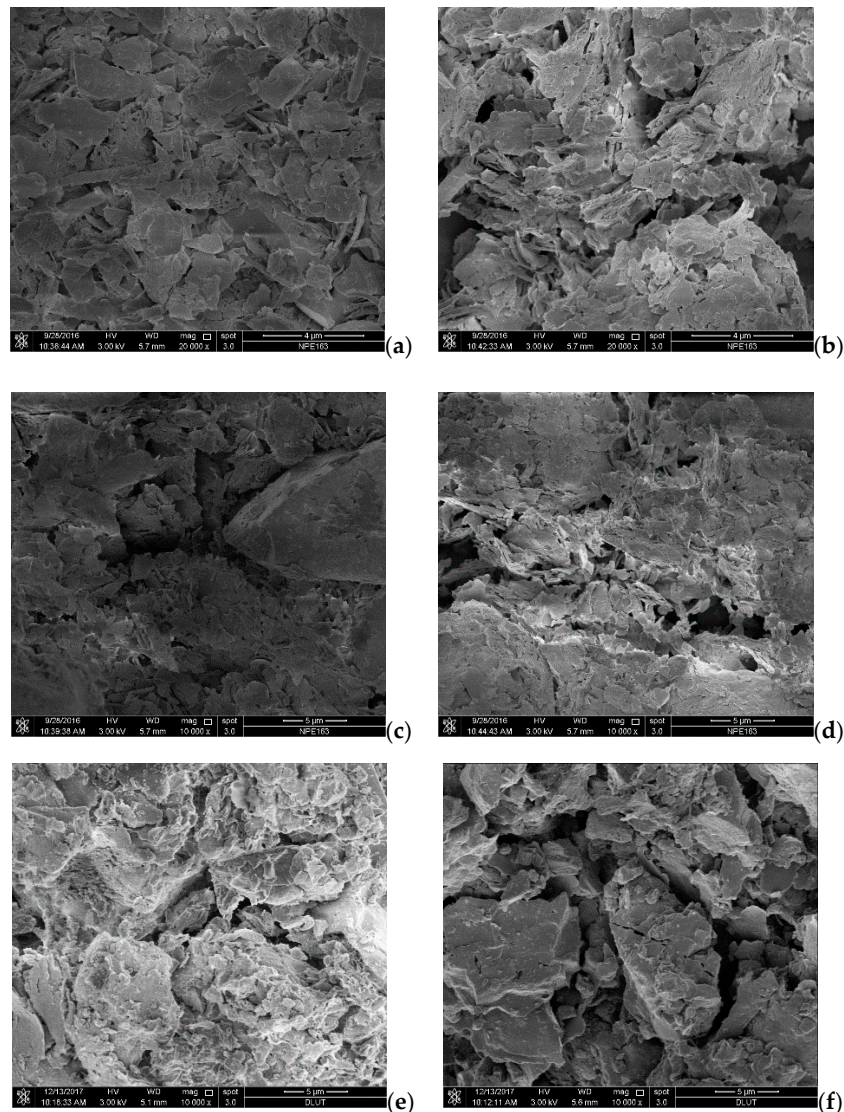
Figure 2. S-1 marine sediments: (a) before remolding; (b) after remolding.

Table 1 shows the drilling depths and particle size distributions of marine sediments. It can be clearly seen that S-1, S-2, S-3 and S-4 marine sediments belong to the same hydrate-bearing layer, while S-5 marine sediments belong to a different hydrate-bearing layer below the seafloor based on the drilling depth. It is obvious that the mean particle size of marine sediments decreases slightly with increasing drilling depth, and S-3 and S-4 marine sediments display a better particle gradation than the other three marine sediments.

Table 1. Drilling depths and particle size distributions of different marine sediments and artificial silt.

Sediments	Particle Size					Mean Size (μm)	Depth (m)
	<1.5 μm	1.5 μm –4 μm	4 μm –10 μm	10 μm –25 μm	>25 μm		
S-1	9.07%	18.71%	31.89%	25.16%	15.17%	9.165	128
S-2	7.83%	20.52%	29.47%	23.6%	18.58%	8.997	132
S-3	14.01%	23.97%	20.81%	20.88%	20.33%	7.976	133
S-4	12.68%	21.18%	20.54%	22.65%	22.95%	7.983	134
S-5	9.99%	20.82%	33.52%	22.34%	13.33%	7.925	158
Artificial silt	11.54%	17.93%	28.99%	24.69%	16.85%	8.270	

In Figure 3, the SEM images of S-1, S-2, S-3, S-4 and S-5 marine sediments and artificial silt prove that these six materials display obviously different aggregate morphology: S-1, S-2 and S-3 marine sediments and artificial silt display a similar, relatively uniform lamella shape while S-4 and S-5 marine sediments mostly present a sticky flocculent shape. It can be observed that there are more coarse soil particles and fine particles in S-3 and S-4 marine sediments, implying that S-3 and S-4 marine sediments have a better particle gradation than the other marine sediments.

**Figure 3.** SEM images of marine sediments: (a) S-1; (b) S-2; (c) S-3; (d) S-4; (e) S-5; (f) artificial silt.

2.3. Sample Preparation and Shear Process

During the sample-remolding process, ice powder (average particle size of 250 μm) was made and placed into a high-pressure reactor. The reactor was then sealed and methane gas of 10 MPa was injected into the reactor to generate CH_4 hydrate in the next 48 h. The hydrate saturation was approximately 30% in this hydrate formation method. Afterwards, according to the pre-designed porosity (40%), a certain amount of hydrate containing ice and marine sediments was weighed, mixed equally and put into the remolding device to form the sample of HBMS (100 mm \times 50 mm). In order to obtain samples with different hydrate saturations, we put pure ice powder into hydrate containing ice to alter the hydrate saturation. To form the interbedded sample, hydrate containing ice and marine sediments was placed into the molding device by turns to form a sample with 11 different layers (Interbedded 1) or 21 different layers (Interbedded 2), as shown in Figure 4. All of the above work was conducted in a cold room ($-20\text{ }^\circ\text{C}$) to reduce hydrate dissociation.

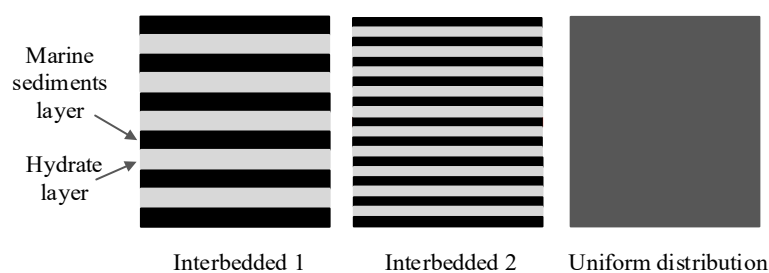


Figure 4. Schematic diagrams of HBMS with different forms of hydrate.

Then the sample was wrapped with a rubber membrane, top platen and bottom platen. The pre-designed effective confining pressure and temperature were adjusted after the sample was transformed vertically in the pressure chamber. After adequate isotropic consolidation, the sample was sheared. In this study, a series of triaxial tests on HBMS were conducted under a confining pressure of 3 MPa, at a strain rate of 1 mm/min and a temperature of 5 $^\circ\text{C}$.

3. Results and Discussion

3.1. Effect of Drilling Depth

Figure 5 shows the stress–strain curves of remolded HBMS at different drilling depths. From the figure, it is clear that all HBMS display strain hardening on the stress–strain curves, occurring over three stages: the elastic–plastic stage, the yield stage and the critical state stage. The maximum stress of HBMS mostly occurs at approximately 7%–8% strain, which is consistent with previous work [26,38,44,56].

A comparison between the mechanical properties of HBMS formed by S-1, S-2, S-3 and S-4 marine sediments in Figure 6 clearly shows that the elastic modulus and failure strength of HBMS S-3 and S-4 are higher than those of other HBMS, which can be explained by the fact that S-3 and S-4 marine sediments have a better particle gradation, as shown in Table 1. For the sediment matrix with a better particle gradation, the number of contact points between large particles and fine particles in the unit volume may increase and enhance the shear strength of HBMS [38,41]. However, it is clear that HBMS S-5 displays lower stiffness and failure strength compared to the other HBMS. Table 1 shows the mean particle size of the marine sediments gradually declines with the increase of drilling depth, which may cause the lower failure strength of HBMS formed by S-5 marine sediments [45,46]. Another reason for this phenomenon is that, as shown by the SEM images of S-5 marine sediments, the soil particles are mostly a sticky flocculent shape. According to Hyodo et al. [38], high effective stress may produce the occurrence of a sticky flocculent shape of soil particles, reducing the failure strength of hydrate-bearing sediments. Hence, for this study, the increase of drilling depth would bring about higher effective stress and lead to the decline of the failure strength in HBMS.

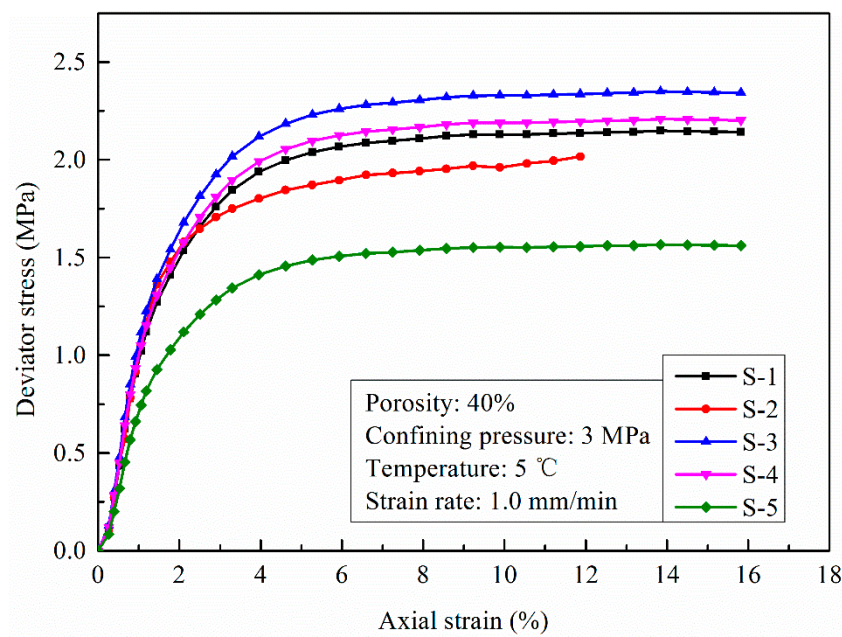


Figure 5. Stress–strain curves of HBMS at different drilling depths.

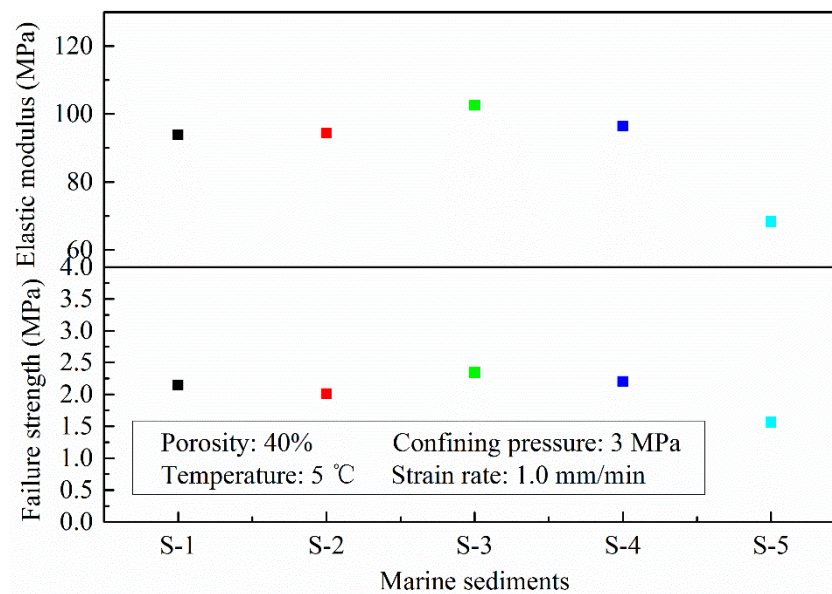


Figure 6. Elastic modulus and failure strength of HBMS at different drilling depths.

The above results show that the decrease of mean particle size and the change in the aggregate morphology of soil particles would decrease the elastic modulus and failure strength of HBMS, and a better particle gradation of marine sediments may effectively enhance the failure strength of HBMS.

To find one possible kind of soil which can replace marine sediments in massive and systematic triaxial shear tests, hydrate-bearing artificial silt and hydrate-bearing kaolin clay were remolded and used for the investigation. The relationships between stress–strain curves and different kinds of soil observed are displayed in Figures 7 and 8. The similar strain hardening phenomenon, elastic modulus and failure strength show that the mechanical characteristics of remolded HBMS and hydrate-bearing clays are nearly consistent. Hence, we suggest that the kaolin clay and artificial silt could be used to investigate the mechanical stability of hydrate reservoirs instead of marine sediments.

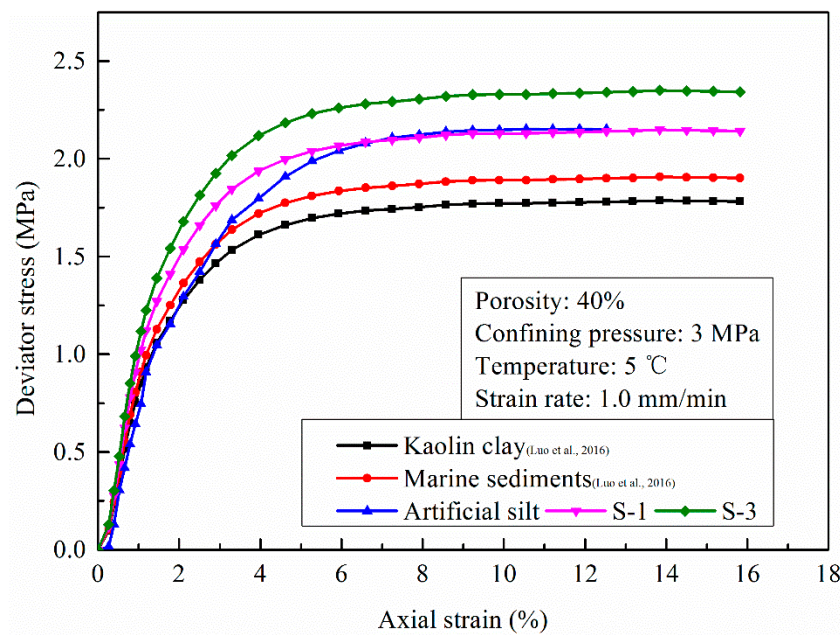


Figure 7. Stress–strain curves of HBMS, hydrate-bearing artificial silt and hydrate-bearing kaolin clay.

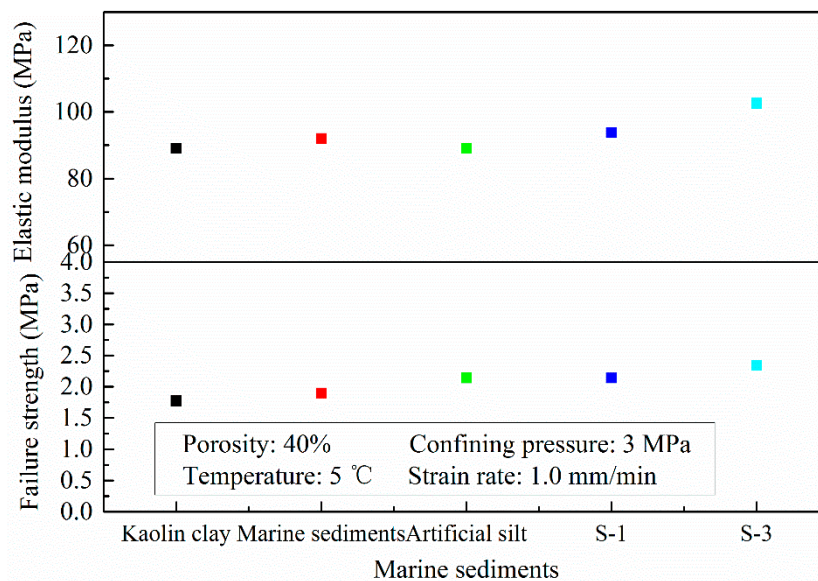


Figure 8. Elastic modulus and failure strength of HBMS, hydrate-bearing artificial silt and hydrate-bearing kaolin clay.

3.2. Effect of Hydrate Saturation and Existence Form of Hydrate

In Figures 9 and 10, the stress–strain curves of HBMS with different hydrate saturations and different existence forms of hydrate all exhibit hyperbola behaviors with strain hardening. Nevertheless, the maximum deviator stress of HBMS changes with hydrate saturation and the existence form of hydrate.

Hyodo et al. [57] suggested that the hydrate saturation level influences the mechanical behaviors of hydrate-bearing sands, and this study confirmed these results for HBMS, as shown in Figure 11a. The figure shows that the failure strength of HBMS increases slightly with the increase of hydrate saturation. Since the mixed sample preparation method was used to remold the HBMS, one can expect most of the hydrate structures would be a pore-filling type or a frame-supporting type. Since the hydrate is already in the solid form when it was mixed with the sediments, no cementation is expected since this occurs only during hydrate formation. Thus, hydrate particles mostly play a partial

load-bearing role in the structure strength, leading to the slight increase of the failure strength of HBMS. Moreover, the relatively small change of HBMS in the interbedded form and uniform distribution form in Figure 11b can also be attributed to the fact that the hydrate structure in HBMS is mostly the pore-filling type or frame-supporting type, preventing cementation between the soil particles. Thus, even the hydrate layers are separated from the marine sediments layers, the failure strength change of HBMS is not so obvious.

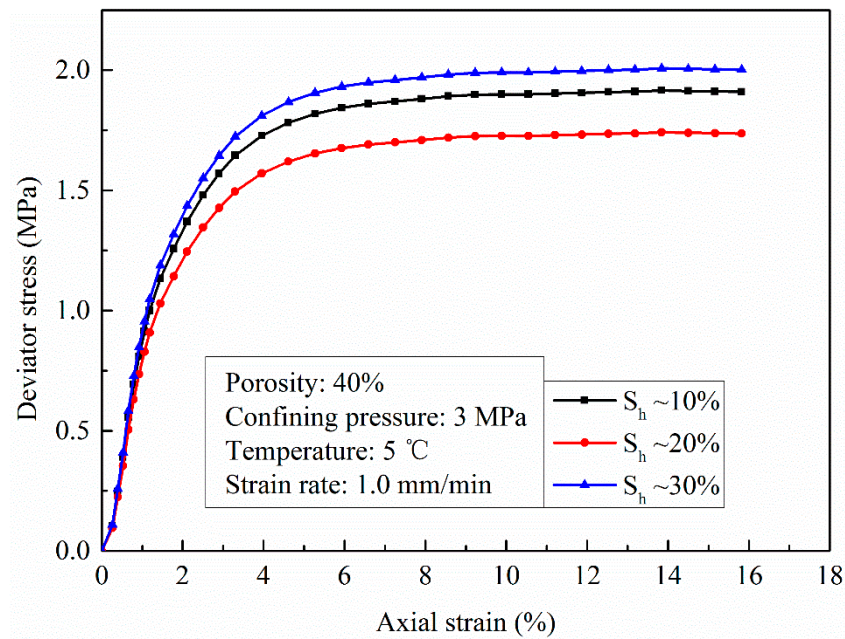


Figure 9. Stress–strain curves of HBMS with different hydrate saturations.

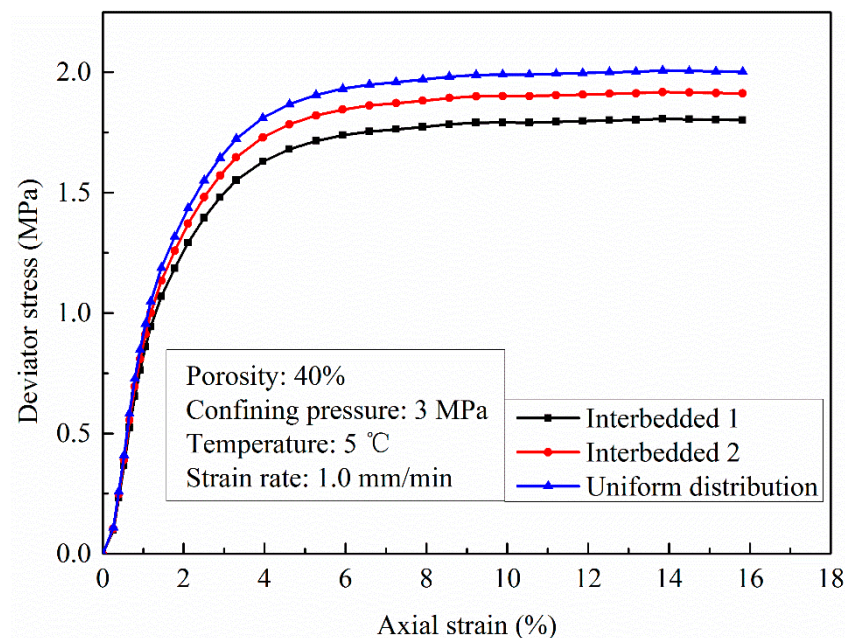


Figure 10. Stress–strain curves of HBMS with different existence forms of hydrate.

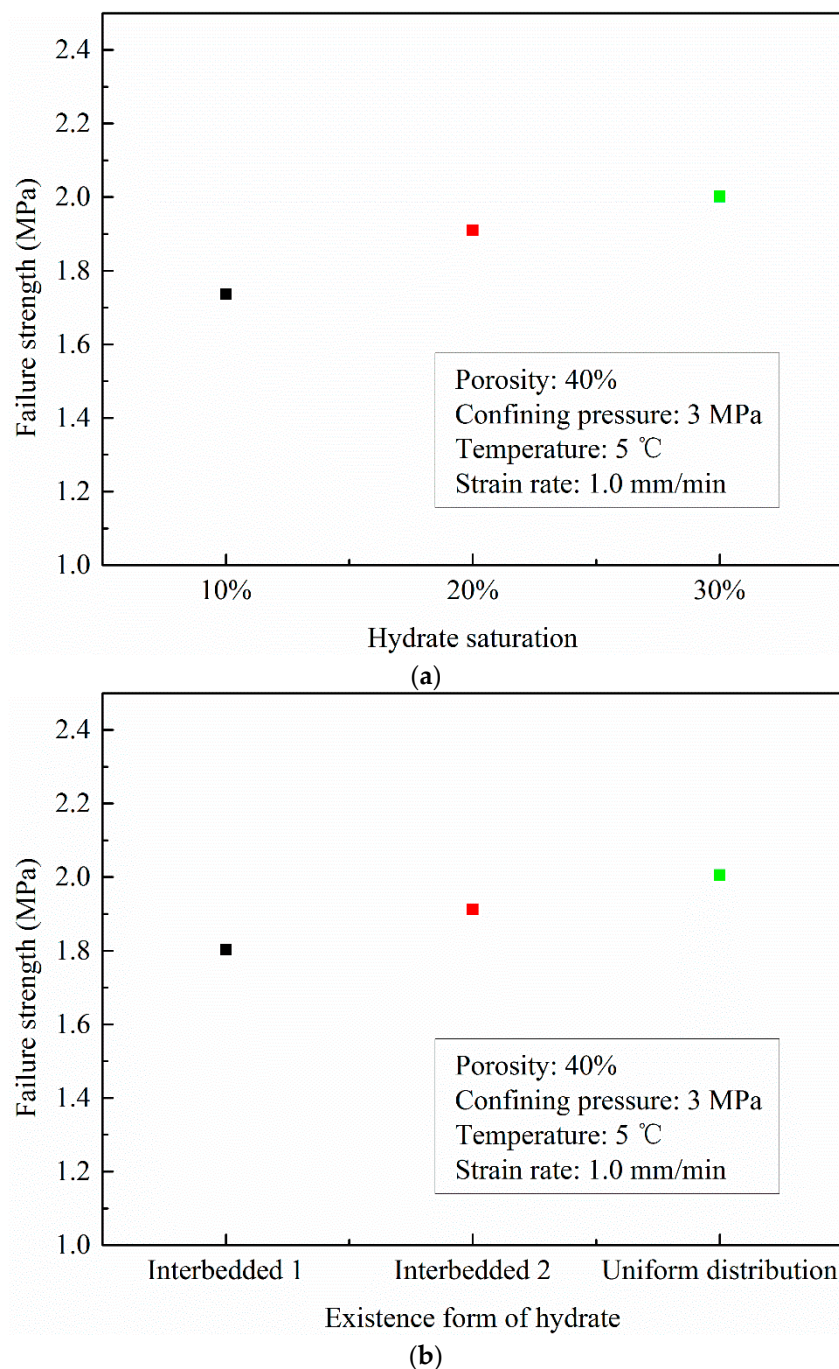


Figure 11. Failure strength of HBMS: (a) with different hydrate saturations; (b) in different existence forms of hydrate.

3.3. Effect of Hydrate Dissociation

Hydrate dissociation has a significant influence on the mechanical properties of hydrate-bearing sediments [21,24]. The data in Figure 12 clearly show the stress–strain curves of HBMS formed by S-1 and S-3 marine sediments before and after hydrate dissociation. All curves present three compression stages: the elastic-plastic stage, the yield stage and the critical state stage, which indicates that hydrate dissociation would not dramatically influence the strain hardening characteristics of HBMS.

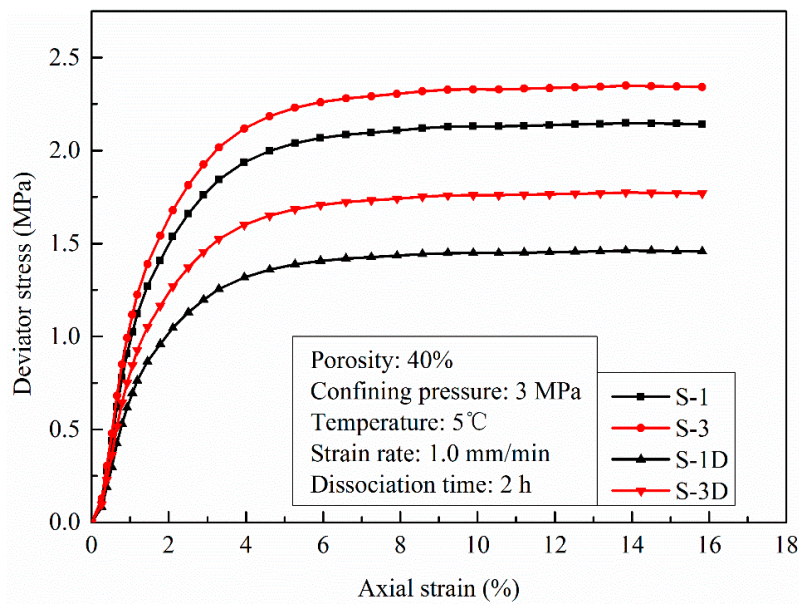


Figure 12. Stress–strain curves of HBMS formed by S-1 and S-3 marine sediments before and after hydrate dissociation.

The data in Figure 13 clearly show that the elastic modulus and failure strength of remolded HBMS formed by S-1 and S-3 marine sediments decline significantly after hydrate dissociation, indicating that hydrate dissociation has a significant influence on the mechanical stability of hydrate reservoirs in the natural gas exploitation process. One reason for this behavior could be that hydrate particles of the pore-filling type or the frame-supporting type in HBMS mostly play a partial load-bearing role in the structure strength of HBMS. Thus, hydrate dissociation would also reduce the structure strength of HBMS due to the hydrate particles having vanished. Moreover, by comparing the data on HBMS formed by S-1 and S-3 marine sediments before and after hydrate dissociation in this figure, it can also be found that the value of the elastic modulus and failure strength decline of remolded HBMS in the same layer are almost consistent after hydrate dissociation. This result may imply that the existence of hydrate works in a similar way on hydrate reservoirs in the same layer.

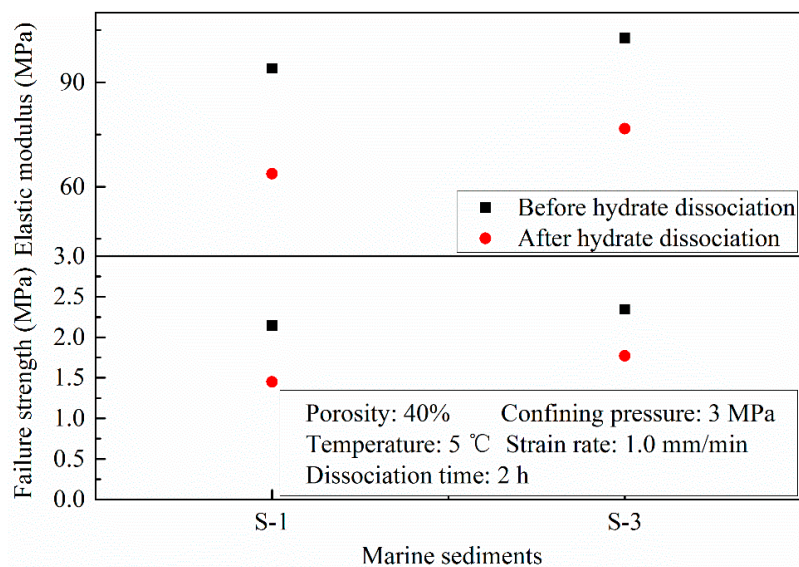


Figure 13. Elastic modulus and failure strength of HBMS formed by S-1 and S-3 marine sediments before and after hydrate dissociation.

4. Conclusions

In this study, a series of triaxial tests was conducted to investigate the effects of soil particle gradation and hydrate existence on the mechanical properties of remolded HBMS.

(1) The stress–strain behaviors of remolded HBMS at different drilling depths are consistent. The elastic modulus and strength properties of HBMS decline with the decrease of the mean particle size and with aggregate morphology changes of the marine sediment particles. In addition, a better particle gradation of marine sediments may effectively enhance the failure strength of HBMS.

(2) The similar strength characteristics of remolded HBMS and hydrate-bearing artificial silt prove that artificial silt can be used as a replacement for marine sediments to investigate the mechanical properties of hydrate reservoirs.

(3) The existence of hydrate plays an important role in the strength behaviors of HBMS. It was found that the failure strength of HBMS increases with increasing hydrate saturation even though most of the hydrate structures are the pore-filling type or frame-supporting type in the mixed sample preparation method. The reduction in the failure strength of HBMS with 30% initial hydrate saturation is more than 35% after complete hydrate dissociation.

Author Contributions: Conceptualization, Y.L. and T.L.; Formal Analysis, Y.L., T.L. and X.S.; Resources, Q.L. and Y.L.; Data Curation, T.L.; Writing-Original Draft Preparation, T.L.; Writing-Review & Editing, Y.L., X.S. and W.L.; Supervision, W.L. and Y.S.; Funding Acquisition, Y.S.

Funding: This research was funded by the National Natural Science Foundation of China (Grant Nos. 51876029 and 51890911), the National Key Research and Development Program of China (Grant Nos. 2017YFC0307305 and 2016YFC0304001), and the Fundamental Research Funds for the Central Universities (Grant No. DUT16RC(4)37).

Conflicts of Interest: The authors declare no conflict of interest.

References

1. Dai, S.; Santamarina, J. Sampling disturbance in hydrate-bearing sediment pressure cores: NGHP-01 expedition, Krishna–Godavari Basin example. *Mar. Pet. Geol.* **2014**, *58*, 178–186. [[CrossRef](#)]
2. Dawe, R.; Thomas, S. A Large Potential Methane Source—Natural Gas Hydrates. *Energy Sources Part A* **2007**, *29*, 217–229. [[CrossRef](#)]
3. Lee, S.; Holder, G. Methane hydrates potential as a future energy source. *Fuel Process. Technol.* **2001**, *71*, 181–186. [[CrossRef](#)]
4. Kuang, Y.; Lei, X.; Yang, L.; Zhao, Y.; Zhao, J. Observation of In Situ Growth and Decomposition of Carbon Dioxide Hydrate at Gas–Water Interfaces Using Magnetic Resonance Imaging. *Energy Fuels* **2018**, *32*, 6964–6969. [[CrossRef](#)]
5. Yang, L.; Ai, L.; Xue, K.; Ling, Z.; Li, Y. Analyzing the effects of inhomogeneity on the permeability of porous media containing methane hydrates through pore network models combined with CT observation. *Energy* **2018**, *163*, 27–37. [[CrossRef](#)]
6. Martens, C.; Mendlovitz, H.; Seim, H.; Lapham, L.; D’Emidio, M. Sustained in situ measurements of dissolved oxygen, methane and water transport processes in the benthic boundary layer at MC118, northern Gulf of Mexico. *Deep Sea Res. Part II* **2016**, *129*, 41–52. [[CrossRef](#)]
7. Rose, K.; Boswell, R.; Collett, T. Mount Elbert Gas Hydrate Stratigraphic Test Well, Alaska North Slope: Coring operations, core sedimentology, and lithostratigraphy. *Mar. Pet. Geol.* **2011**, *28*, 311–331. [[CrossRef](#)]
8. Usapkar, A.; Dewangan, P.; Kocherla, M.; Ramprasad, T.; Mazumdar, A.; Ramana, M. Enhanced methane flux event and sediment dispersal pattern in the Krishna–Godavari offshore basin: Evidences from rock magnetic techniques. *Mar. Pet. Geol.* **2014**, *58*, 461–475. [[CrossRef](#)]
9. Yoneda, J.; Masui, A.; Konno, Y.; Jin, Y.; Egawa, K.; Kida, M.; Ito, T.; Nagao, J.; Tenma, N. Mechanical behavior of hydrate-bearing pressure-core sediments visualized under triaxial compression. *Mar. Pet. Geol.* **2015**, *66*, 451–459. [[CrossRef](#)]
10. Li, G.; Moridis, G.J.; Zhang, K.; Li, X. Evaluation of gas production potential from marine gas hydrate deposits in Shenhu area of South China Sea. *Energy Fuels* **2010**, *24*, 6018–6033. [[CrossRef](#)]

11. Li, G.; Moridis, G.J.; Zhang, K.; Li, X. The use of huff and puff method in a single horizontal well in gas production from marine gas hydrate deposits in the Shenhu Area of South China Sea. *J. Pet. Sci. Eng.* **2011**, *77*, 49–68. [[CrossRef](#)]
12. Sun, J.; Zhang, L.; Ning, F.; Lei, W.; Liu, L.; Hu, W.; Lu, H.; Lu, J.; Liu, C.; Jiang, G.; et al. Production potential and stability of hydrate-bearing sediments at the site GMGS3-W19 in the South China Sea: A preliminary feasibility study. *Mar. Pet. Geol.* **2017**, *86*, 447–473. [[CrossRef](#)]
13. Brown, H.; Holbrook, W.; Hornbach, M.; Nealon, J. Slide structure and role of gas hydrate at the northern boundary of the Storegga Slide, offshore Norway. *Mar. Geol.* **2006**, *229*, 179–186. [[CrossRef](#)]
14. Clayton, C.R.I.; Priest, J.A.; Rees, E.V.L. The effects of hydrate cement on the stiffness of some sands. *Géotechnique* **2010**, *60*, 435–445. [[CrossRef](#)]
15. Kim, Y.; Lee, S.; Jin, Y.; Baranov, B.; Obzhairov, A.; Salomatin, A.; Shoji, H. The stability of gas hydrate field in the northeastern continental slope of Sakhalin Island, Sea of Okhotsk, as inferred from analysis of heat flow data and its implications for slope failures. *Mar. Pet. Geol.* **2013**, *45*, 198–207. [[CrossRef](#)]
16. Kvenvolden, K.; Ginsburg, G.; Soloviev, V. Worldwide distribution of subaquatic gas hydrates. *Geo-Mar. Lett.* **1993**, *13*, 32–40. [[CrossRef](#)]
17. Sun, X.; Guo, X.; Shao, L.; Tang, H. A thermodynamics-based critical state constitutive model for methane hydrate bearing sediment. *J. Nat. Gas Sci. Eng.* **2015**, *27*, 1024–1034. [[CrossRef](#)]
18. Sun, X.; Hao, L.; Soga, K. A coupled thermal–hydraulic–mechanical–chemical (THMC) model for methane hydrate bearing sediments using COMSOL Multiphysics. *J. Zhejiang Univ. Sci. A* **2018**, *19*, 600–623. [[CrossRef](#)]
19. Grozic, J.; Ghiassian, H. Undrained shear strength of methane hydrate-bearing sand; preliminary laboratory results. In Proceedings of the 6th Canadian permafrost conference and 63rd Canadian geotechnical conference, Calgary, CA, USA, 12–16 September 2010; pp. 459–466.
20. Hyodo, M.; Nakata, Y.; Yoshimoto, N.; Fukunaga, M.; Kubo, K.; Nanjo, Y.; Matsuo, T.; Nakamura, K. Triaxial Compressive Strength of Methane Hydrate. In Proceedings of the International Offshore and Polar Engineering Conference, Kitakyushu, Japan, 26–31 May 2002.
21. Hyodo, M.; Nakata, Y.; Yoshimoto, N.; Yoneda, J. Shear strength of methane hydrate bearing sand and its deformation during dissociation of methane hydrate. In Proceedings of the 4th International Symposium on Deformation Characteristics of Geomaterials, Georgia, GA, USA, 15 September 2008; pp. 549–556.
22. Hyodo, M.; Nakata, Y.; Yoshimoto, N.; Orense, R.; Yoneda, J.; Nakagawa, M.; Luding, S. Bonding Strength by Methane Hydrate Formed among Sand Particles. *AIP Conf. Proc.* **2009**, *1145*, 79–82.
23. Hyodo, M.; Li, Y.; Yoneda, J.; Nakata, Y.; Yoshimoto, N.; Nishimura, A.; Song, Y. Mechanical behavior of gas-saturated methane hydrate-bearing sediments. *J. Geophys. Res.* **2013**, *118*, 5185–5194. [[CrossRef](#)]
24. Hyodo, M.; Li, Y.; Yoneda, J.; Nakata, Y.; Yoshimoto, N.; Nishimura, A. Effects of dissociation on the shear strength and deformation behavior of methane hydrate-bearing sediments. *Mar. Pet. Geol.* **2014**, *51*, 52–62. [[CrossRef](#)]
25. Li, Y.; Liu, W.; Zhu, Y.; Chen, Y.; Song, Y.; Li, Q. Mechanical behaviors of permafrost-associated methane hydrate-bearing sediments under different mining methods. *Appl. Energy* **2016**, *162*, 1627–1632. [[CrossRef](#)]
26. Li, Y.; Song, Y.; Liu, W.; Yu, F. Experimental research on the mechanical properties of methane hydrate-ice mixtures. *Energies* **2012**, *5*, 181–192. [[CrossRef](#)]
27. Li, Y.; Song, Y.; Yu, F.; Liu, W.; Zhao, J. Experimental study on mechanical properties of gas hydrate-bearing sediments using kaolin clay. *China Ocean Eng.* **2011**, *25*, 113–122. [[CrossRef](#)]
28. Liu, W.; Li, Y.; Xu, X.; Song, Y. Study on Influence Factors of Methane Hydrate Formation from Ice: Temperature, Pressure and SDS Surfactant. *Chin. J. Chem. Eng.* **2018**. [[CrossRef](#)]
29. Liu, W.; Luo, T.; Li, Y.; Song, Y.; Zhu, Y.; Liu, Y.; Zhao, J.; Wu, Z.; Xu, X. Experimental study on the mechanical properties of sediments containing CH₄ and CO₂ hydrate mixtures. *J. Nat. Gas Sci. Eng.* **2016**, *32*, 20–27. [[CrossRef](#)]
30. Liu, W.; Wu, Z.; Li, Y.; Song, Y.; Ling, Z.; Zhao, J.; Lv, Q. Experimental study on the gas phase permeability of methane hydrate-bearing clayey sediments. *J. Nat. Gas Sci. Eng.* **2016**, *36*, 378–384. [[CrossRef](#)]
31. Miyazaki, K.; Masui, A.; Aoki, K.; Sakamoto, Y.; Yamaguchi, T.; Okubo, S. Strain-rate dependence of triaxial compressive strength of artificial methane-hydrate-bearing sediment. *Int. J. Offshore Polar Eng.* **2010**, *20*.
32. Miyazaki, K.; Masui, A.; Sakamoto, Y.; Aoki, K.; Tenma, N.; Yamaguchi, T. Triaxial compressive properties of artificial methane-hydrate-bearing sediment. *J. Geophys. Res.* **2011**, *116*. [[CrossRef](#)]

33. Miyazaki, K.; Tenma, N.; Aoki, K.; Sakamoto, Y.; Yamaguchi, T. Effects of confining pressure on mechanical properties of artificial methane-hydrate-bearing sediment in triaxial compression test. *Int. J. Offshore Polar Eng.* **2011**, *21*.
34. Wu, Z.; Li, Y.; Sun, X.; Li, M.; Jia, R. Experimental study on the gas phase permeability of montmorillonite sediments in the presence of hydrates. *Mar. Pet. Geol.* **2018**, *91*, 373–380. [[CrossRef](#)]
35. Wu, Z.; Li, Y.; Sun, X.; Wu, P.; Zheng, J. Experimental study on the effect of methane hydrate decomposition on gas phase permeability of clayey sediments. *Appl. Energy* **2018**, *230*, 1304–1310. [[CrossRef](#)]
36. Grozic, J. *Interplay between Gas Hydrates and Submarine Slope Failure, Submarine Mass Movements and Their Consequences*; Springer: Berlin, Germany, 2010; pp. 11–30.
37. Hyodo, M.; Nishimura, A.; Kajiyama, S. Effect of fines on shear strength of methane hydrate bearing sand. In Proceedings of the Eleventh Ocean Mining and Gas Hydrates Symposium, Kona, HI, USA, 21–27 June 2015.
38. Luo, T.; Li, Y.; Liu, W.; Sun, X.; Shen, S. Experimental Study on the Mechanical Properties of CH₄ and CO₂ Hydrate Remodeling Cores in Qilian Mountain. *Energies* **2017**, *10*, 2078. [[CrossRef](#)]
39. Luo, T.; Li, Y.; Sun, X.; Shen, S.; Wu, P. Effect of sediment particle size on the mechanical properties of CH₄ hydrate-bearing sediments. *J. Pet. Sci. Eng.* **2018**, *171*, 302–314. [[CrossRef](#)]
40. Madhusudhan, B.N.; Clayton, C.; Priest, J.A. The effects of hydrate on the strength and stiffness of some sands. *J. Geophys. Res.* **2018**. [[CrossRef](#)]
41. Miyazaki, K.; Tenma, N.; Aoki, K.; Yamaguchi, T. A Nonlinear Elastic Model for Triaxial Compressive Properties of Artificial Methane-Hydrate-Bearing Sediment Samples. *Energies* **2012**, *5*, 4057–4075. [[CrossRef](#)]
42. Yoneda, J.; Hyodo, M.; Yoshimoto, N.; Nakata, Y.; Kato, A. Development of high-pressure low-temperature plane strain testing apparatus for methane hydrate-bearing sand. *Soils Found.* **2013**, *53*, 774–783. [[CrossRef](#)]
43. Yoneda, J.; Masui, A.; Konno, Y.; Jin, Y.; Egawa, K.; Kida, M.; Ito, T.; Nagao, J.; Tenma, N. Mechanical properties of hydrate-bearing turbidite reservoir in the first gas production test site of the Eastern Nankai Trough. *Mar. Pet. Geol.* **2015**, *66*, 471–486. [[CrossRef](#)]
44. Yun, T.; Santamarina, J.; Ruppel, C. Mechanical properties of sand, silt, and clay containing tetrahydrofuran hydrate. *J. Geophys. Res.* **2007**, *112*. [[CrossRef](#)]
45. Masui, A.; Haneda, H.; Ogata, Y.; Aoki, K. Effects of methane hydrate formation on shear strength of synthetic methane hydrate sediments. In Proceedings of the Fifteenth International Offshore and Polar Engineering Conference, Seoul, Korea, 19–24 June 2005.
46. Masui, A.; Haneda, H.; Ogata, Y.; Aoki, K. Mechanical properties of sandy sediment containing marine gas hydrates in deep sea offshore Japan. In Proceedings of the Seventh ISOPE Ocean Mining Symposium, Lisbon, Portugal, 1–6 July 2007.
47. Winters, W.; Wilcox-Cline, R.; Long, P.; Dewri, S.; Kumar, P.; Stern, L.; Kerr, L. Comparison of the physical and geotechnical properties of gas-hydrate-bearing sediments from offshore India and other gas-hydrate-reservoir systems. *Mar. Pet. Geol.* **2014**, *58*, 139–167. [[CrossRef](#)]
48. Hyodo, M.; Nakata, Y.; Yoshimoto, N.; Kbimuna, T. Basic research on the mechanical behavior of methane hydrate-sediments mixture. *J. Jpn. Geotech. Soc.* **2005**, *45*, 75–85.
49. Hyodo, M.; Yoneda, J.; Yoshimoto, N.; Nakata, Y. Mechanical and dissociation properties of methane hydrate-bearing sand in deep seabed. *Soils Found.* **2013**, *53*, 299–314. [[CrossRef](#)]
50. Yoneda, J.; Masui, A.; Konno, Y.; Jin, Y.; Kida, M.; Katagiri, J.; Nagao, J.; Tenma, N. Pressure-core-based reservoir characterization for geomechanics: Insights from gas hydrate drilling during 2012–2013 at the eastern Nankai Trough. *Mar. Pet. Geol.* **2017**, *86*, 1–16. [[CrossRef](#)]
51. Luo, T.; Song, Y.; Zhu, Y.; Liu, W.; Liu, Y.; Li, Y.; Wu, Z. Triaxial experiments on the mechanical properties of hydrate-bearing marine sediments of South China Sea. *Mar. Pet. Geol.* **2016**, *77*, 507–514. [[CrossRef](#)]
52. Priest, J.; Clayton, C.; Rees, E. Potential impact of gas hydrate and its dissociation on the strength of host sediment in the Krishna–Godavari Basin. *Mar. Pet. Geol.* **2014**, *58*, 187–198. [[CrossRef](#)]
53. Yun, T.; Fratta, D.; Santamarina, J. Hydrate-Bearing Sediments from the Krishna–Godavari Basin: Physical Characterization, Pressure Core Testing, and Scaled Production Monitoring. *Energy Fuels* **2010**, *24*, 5972–5983. [[CrossRef](#)]
54. Liu, C.; Ye, Y.; Meng, Q.; He, X.; Lu, H.; Zhang, J.; Liu, J.; Yang, S. The characteristics of gas hydrates recovered from Shenhu Area in the South China Sea. *Mar. Geol.* **2012**, *307*, 22–27. [[CrossRef](#)]

55. Miyazaki, K.; Tenma, N.; Aoki, K.; Sakamoto, Y.; Yamaguchi, T. Loading-Rate Dependence of Triaxial Compressive Strength of Artificial Methane-Hydrate-Bearing Sediment Containing Fine Fraction. In Proceedings of the International Society of Offshore and Polar Engineers, Rhodes, Greece, 26 June–1 July 2012; pp. 17–22.
56. Yu, F.; Song, Y.; Liu, W.; Li, Y.; Lam, W. Analyses of stress strain behavior and constitutive model of artificial methane hydrate. *J. Pet. Sci. Eng.* **2011**, *77*, 183–188. [[CrossRef](#)]
57. Hyodo, M.; Li, Y.; Yoneda, J.; Nakata, Y.; Yoshimoto, N.; Kajiyama, S.; Nishimura, A.; Song, Y. A comparative analysis of the mechanical behavior of carbon dioxide and methane hydrate-bearing sediments. *Am. Mineral.* **2014**, *99*, 178–183. [[CrossRef](#)]



© 2019 by the authors. Licensee MDPI, Basel, Switzerland. This article is an open access article distributed under the terms and conditions of the Creative Commons Attribution (CC BY) license (<http://creativecommons.org/licenses/by/4.0/>).